PNAS RESEARCH ARTICLE | EARTH, ATMOSPHERIC, AND PLANETARY SCIENCES OPEN ACCESS

Highly enriched carbon and oxygen isotopes in carbonate-derived CO_2 at Gale crater, Mars

David G. Burtt[a,1], Jennifer C. Stern[b], Christopher R. Webster[c], Amy E. Hofmann[c], Heather B. Franz[b], Brad Sutter[d,e], Michael T. Thorpe[b,f], Edwin S. Kite[g], Jennifer L. Eigenbrode[b], Alexander A. Pavlov[b], Christopher H. House[h], Benjamin M. Tutolo[i], David J. Des Marais[j], Elizabeth B. Rampe[e], Amy C. McAdam[b], and Charles A. Malespin[b]

Affiliations are included on p. 9.

Edited by John Eiler, California Institute of Technology, Pasadena, CA; received January 8, 2024; accepted August 7, 2024

Carbonate minerals are of particular interest in paleoenvironmental research as they are an integral part of the carbon and water cycles, both of which are relevant to habitability. Given that these cycles are less constrained on Mars than they are on Earth, the identification of carbonates has been a point of emphasis for rover missions. Here, we present carbon ($\delta^{13}C$) and oxygen ($\delta^{18}O$) isotope data from four carbonates encountered by the Curiosity rover within the Gale crater. The carbon isotope values range from 72 ± 2‰ to 110 ± 3‰ Vienna Pee Dee Belemnite while the oxygen isotope values span from 59 ± 4‰ to 91 ± 4‰ Vienna Standard Mean Ocean Water (1 SE uncertainties). Notably, these values are isotopically heavy (^{13}C- and ^{18}O-enriched) relative to nearly every other Martian material. The extreme isotopic difference between the carbonates and other carbon- and oxygen-rich reservoirs on Mars cannot be reconciled by standard equilibrium carbonate–CO_2 fractionation, thus requiring an alternative process during or prior to carbonate formation. This paper explores two processes capable of contributing to the isotopic enrichments: 1) evaporative-driven Rayleigh distillation and 2) kinetic isotope effects related to cryogenic precipitation. In isolation, each process cannot reproduce the observed carbonate isotope values; however, a combination of these processes represents the most likely source for the extreme isotopic enrichments.

Mars | carbon isotopes | oxygen isotopes | Gale crater | carbonate

Significance

One objective of the Curiosity rover is to search for habitable conditions, past and present, on the surface of Mars. Carbonate minerals can record diagnostic signatures of their formation environment. This paper focuses on carbon and oxygen isotope measurements of carbonate minerals detected within the Gale crater. Notably, these carbonates are extremely enriched in ^{13}C and ^{18}O, more so than other Martian materials. We highlight two processes (evaporation-driven Rayleigh distillation and cryogenic precipitation) that could explain these isotopic enrichments and explore whether those processes are consistent with our current understanding of Mars. These isotopic values offer a poignant example of how the Martian carbon cycle differs from that on Earth without the influences of a biosphere.

Carbon is essential for life and for planetary climate regulation, so understanding its potential reservoirs and fluxes is critical to evaluating the habitability of Mars (1–3). Carbonates are one known reservoir for carbon on Mars, having been detected both at the surface (4–11) and in Mars meteorites (12–16). While carbonates exist on Mars, the detected concentrations are unexpectedly low given that carbonates are an expected weathering product of abundant basaltic lithologies in the presence of a CO_2-rich atmosphere and liquid water (16). This disparity raises questions about how these carbonates formed and how much of a role these minerals played in sequestering CO_2 on Mars. Hypotheses for the origin(s) of these carbonates range from evaporative precipitation (6, 10, 17), supersaturation within lakes or playas (5, 10, 17, 18), groundwater mixing (11), carbonation of peridotite (5, 10, 19), hydrothermal mineralization (5–7, 17, 19), to ultramafic vein-hosted precipitation (5, 17). As these mechanisms demonstrate, carbonates form in direct contact with the carbon and water cycles, which are both necessary for habitability. Furthermore, carbonates can preserve signatures of their source materials and formation conditions, including temperature (20, 21), pH (22), and pCO_2 (23). Such data are crucial for understanding the ancient climates and habitability of Mars (24).

Stable isotope geochemistry can clarify the paleoenvironmental information recorded within carbonates. Carbon and oxygen isotope ratios, expressed as $\delta^{13}C$ and $\delta^{18}O$, respectively, are dependent on the isotopic composition of source materials and any processes that result in fractionation (i.e., the partitioning of isotopes between two or more phases in a system). In the case of carbonates, the primary source materials are H_2O and dissolved CO_2, whose isotopic compositions in turn carry fingerprints of their provenance and processes operating on volatile reservoirs on Mars. Therefore, as carbonates are connected to both the carbon and water cycles, the isotopic composition of these carbonates can be used to identify the source materials, fractionating processes, and environmental conditions (e.g., temperature, pH, and salinity) relevant to these cycles on Mars.

Gale crater was selected as the landing site for the Mars Science Laboratory (MSL) Curiosity rover based in part on orbital observations of mineral assemblages that may reflect global-scale changes in climate (25). The lower units within the stratigraphy follow an upward transition from fluvial-lacustrine to aeolian-dominated deposits, indicating

The authors declare no competing interest.

This article is a PNAS Direct Submission.

Copyright © 2024 the Author(s). Published by PNAS. This open access article is distributed under Creative Commons Attribution-NonCommercial-NoDerivatives License 4.0 (CC BY-NC-ND).

[1]To whom correspondence may be addressed. Email: david.g.burtt@nasa.gov.

This article contains supporting information online at https://www.pnas.org/lookup/suppl/doi:10.1073/pnas.2321342121/-/DCSupplemental.

Published October 7, 2024.

Downloaded from https://www.pnas.org by 71.228.158.19 on April 25, 2025 from IP address 71.228.158.19.

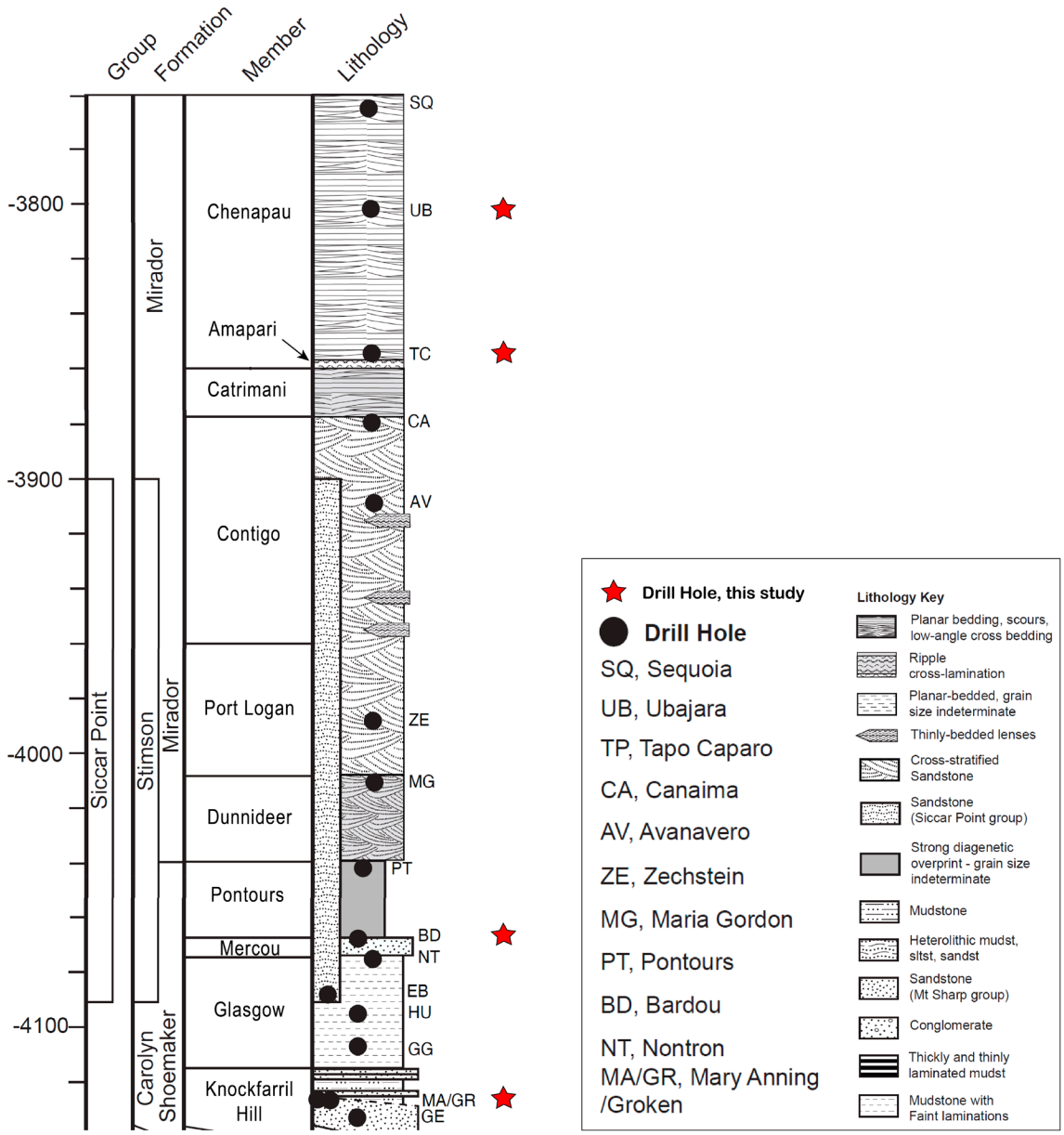

Fig. 1. A select subset of the stratigraphy within Gale crater that includes the four drill sites of interest for this study: MA, BD, TC, and UB. MA and BD were both drilled from fine-grained mudstones and siltstones that have been linked with fluvial-lacustrine activity while TC and UB sit above the Amapari Marker Band in cross-bedded sandstones associated with aeolian environments. The scale bar to the *Left* is measured in meters. Abbreviations in the lithology key include mudst (mudstone), sltst (siltstone), and sandst (sandstone).

that there was a shift from wetter to more arid conditions (25–28). To this point, there have been only scarce orbital (29) and in situ (11, 30–32) measurements to suggest that carbonates are present within the clay- and sulfate-rich units in Gale crater, even though measurements on Earth demonstrate that carbonates can form alongside clay minerals and sulfates on Earth (19, 33). However, the Chemistry & Mineralogy (CheMin) instrument aboard Curiosity recently detected carbonates at multiple drill locations within these stratigraphic units (11, 34). Of these locations, four have corresponding isotopic data: Mary Anning (MA), Bardou (BD), Tapo Caparo (TC), and Ubajara (UB) (32) (Fig. 1). These drill sites span the transition from mixed clay minerals and sulfates (MA and BD), which represent wetter conditions, to sulfates without clay minerals (TC and UB), which reflect a more arid environment. These four drill sites record the highest carbonate abundances detected to this point in Gale crater, suggesting that these carbonates are a significant component of the stratigraphic section and climate. Given this geochemical significance, the Sample Analysis at Mars (SAM) instrument suite analyzed the carbon and oxygen isotopic compositions of the CO_2 evolved during pyrolysis of these rock powders. Here, we present these results and discuss potential mechanisms to explain the isotopic enrichments in the carbonates with respect to known carbon and oxygen reservoirs on Mars.

Results

Drilled samples were pyrolyzed in the SAM oven and the resulting gases were analyzed with the tunable laser spectrometer (TLS), which is described below in the *Materials and Methods* section. No evolved O_2 was detected from these samples as all *m/z* 32 signals were generated by the fragmentation of other compounds. It is therefore unlikely that the measured CO_2 is the product of oxidation of reduced carbon species within samples or the SAM

Downloaded from https://www.pnas.org by 71.228.158.19 on April 25, 2025 from IP address 71.228.158.19.

Table 1. Carbon and oxygen isotope results from carbonate-derived CO_2 taken from four drill samples in Gale crater on Mars

Sample ID	n	$\delta^{13}C$ (‰, VPDB)	$\delta^{13}C$ (1 SE)	$\delta^{18}O$ (‰, VSMOW)	$\delta^{18}O$ (1 SE)	Temperature cut (°C)	Sample depth (m)
Ubajara (UB)	3	96	3	77	3	353 to 553	−3,826
Tapo Caparo (TC)	4	110	3	65	5	353 to 555	−3,854
Bardou (BD)	4	83	3	91	4	301 to 546	−4,066
Mary Anning (MA)	4	72	2	59	4	265 to 552	−4,128

background. The $\delta^{13}C$ and $\delta^{18}O$ values of CO_2, measured by the TLS, are listed in Table 1 with associated precisions of ±1 SE. Carbon isotope values measured by the TLS are reported relative to the Vienna Pee Dee Belemnite (VPDB) standard while oxygen isotope values are reported relative to Vienna Standard Mean Ocean Water (VSMOW). TLS CO_2 isotope data reduction is described in Webster et al. (35). For all data presented here, a minor correction is made: Gas temperatures used have been reduced by ~1 °C by using the cell heater temperature values and the ramp shape that better matches the spectra and thereby reduces errors on the isotope ratio precisions. The source of the CO_2 was determined to be siderite ($FeCO_3$) and ankerite ($Ca\{Fe, Mg, Mn\}\{CO_3\}_2$) based upon mineral identification from CheMin as well as the temperature ranges at which the CO_2 evolved (Tables 1 and 2 and *SI Appendix*, Fig. S1 *A–D*). Previous work (31, 36) shows that crystalline Fe-carbonates will evolve CO_2 between ~500 and 650 °C under SAM oven-like conditions. The CO_2 peaks from this study occur at ~400 °C (*SI Appendix*, Fig. S1 *A–D*), consistent with experimental results examining carbonates with lower degrees of crystallinity (11, 37). Pyrolysis of other phases can produce CO_2 at these temperatures (31, 38) so the combination of CO_2 evolution temperatures and CheMin analysis is necessary to determine that the CO_2 and the resulting $\delta^{13}C$ and $\delta^{18}O$ values come from carbonates. Based on the CheMin analysis, which is described further below in the *Materials and Methods* section, the four drill samples have distinct mineralogical profiles (Table 2). All four sites have abundant plagioclase (14.8 ± 4.1% to 31.2 ± 4.1%) and amorphous components (27.0 ± 20.0% to 60.1 ± 11.5%) with varying amounts of carbonate (0.7 ± 0.9% to 10.8 ± 1.3%). Notably, only MA (28.7 ± 10.0%) and BD (12.0 ± 6.0%) have phyllosilicates. The remaining components consist of pyroxene, hematite, sulfates, and K-feldspar.

The $\delta^{13}C$ and $\delta^{18}O$ values of the CO_2 generated and subsequently analyzed at each of the four sites are listed in Table 1 and shown visually in Fig. 2. MA has the lowest $\delta^{13}C$ and $\delta^{18}O$ values of 72 ± 2‰ and 59 ± 4‰, respectively. Moving upward in the stratigraphy, BD has $\delta^{13}C$ = 83 ± 3‰ and $\delta^{18}O$ = 91 ± 4‰. TC has the highest $\delta^{13}C$ value (110 ± 3‰) with a relatively low $\delta^{18}O$ (65 ± 5‰) compared to the other three samples. Last, UB has $\delta^{13}C$ = 96 ± 3‰ and $\delta^{18}O$ = 77 ± 3‰. These four samples span a ~40‰ range in $\delta^{13}C$ and a ~30‰ range in $\delta^{18}O$, which is even more striking given the limited distance between the samples (~400 m in elevation).

Discussion

Two primary aspects of the carbonate isotope data require explanation: 1) the high $\delta^{13}C$ and $\delta^{18}O$ values relative to all previous $\delta^{13}C$ and $\delta^{18}O$ measurements of Martian materials and 2) the range in $\delta^{13}C$ and $\delta^{18}O$ values across the four samples. To set the stage, we first discuss the existing carbon and oxygen isotope data measured in other reservoirs on Mars.

The dominant carbon species in the modern Martian atmosphere is CO_2 with minor contributions from CO [there are also reports of trace amounts of ephemeral CH_4 (35, 39, 40)]. Modern atmospheric CO_2 [$\delta^{13}C$ = 46 ± 4‰ and $\delta^{18}O$ = 48 ± 5‰ [1 SE] (35)] is enriched in ^{13}C compared to terrestrial tropospheric CO_2 [$\delta^{13}C$ ~ −6‰ preindustrial revolution (41)] but is comparable to the same reservoir in terms of its oxygen isotopic composition ($\delta^{18}O$ ~ 41‰) (42). Two of the leading hypotheses to explain isotopic enrichment in the modern martian atmosphere include atmospheric loss and photolytic dissociation of CO_2. Following the loss of Mars' magnetic dynamo, isotopically light gases were preferentially removed from the atmosphere, leaving the residual gases with lower overall abundance but relative enrichment in heavy isotopes (43). This atmospheric loss is well documented (43, 44), but it is unclear whether this process began early enough to have had a measurable effect on the carbonates in Gale crater. This is contrasted by photolytic dissociation of CO_2 in the atmosphere, which could have occurred at any stage of Martian history and would have enriched the residual CO_2 pool in ^{18}O (45). Loss and associated isotopic fractionation via these processes would be buffered by injections of volcanic material (46) and exchange with the lithosphere (47), although the relative impact of these buffers is not known.

Modern atmospheric CO_2 is significantly ^{13}C-enriched in comparison to igneous macromolecular carbon in a Martian meteorite, which shows a lower $\delta^{13}C$ value of −19.8 ± 4.3‰ (48, 49), perhaps corresponding to magmatic carbon. Spanning the gap between these two endmembers are carbonates hosted within the shergottite, nakhlite, and chassignite (SNC) meteorites, which range in $\delta^{13}C$ from −20.0 ± 0.1 to 49 ± 0.5‰ and in $\delta^{18}O$ from 3.2 ± 0.1 to 25.1 ± 0.7‰ (1, 12, 50). The SNC carbonates have been interpreted to represent magmatic carbon on Mars, with carbonate formation via aqueous alteration due to near-surface hydrothermal activity <1 Ga (51, 52). However, the sedimentary sequences at Gale crater are much older with depositional ages between 3.6 and 3.2 Ga (53), making direct comparisons to the much younger SNC meteorites less robust. K–Ar dating of jarosite samples from the Mojave mudstone point to groundwater infiltration at Gale during the Amazonian, possibly as early as ~2.5 Ga (54). Two martian meteorites, NWA 7034 [2.089 ± 0.081 Ga (55)] and ALH84001 [4.091 ± 0.030 Ga (56)], have radiometric ages that bracket the Gale depositional and infiltration ages, and thus, the isotopic compositions of volatile species in these meteorites may be more relevant comparisons to the volatiles sampled at Gale crater. ALH84001 carbonates have $\delta^{13}C$ = −10.6 ± 0.1 to 64.7 ± 4.2‰ and $\delta^{18}O$ = −5.1 ± 0.1 to 37.2 ± 0.1‰ (12, 50, 57, 58) while bulk C in NWA 7034 has $\delta^{13}C$ = −23.4 ± 0.73‰ (55). NWA 7034 is the most water-rich Martian meteorite identified to date with $\delta^{18}O_{water}$ = −21.78 ± 0.05 to 11.02 ± 0.04‰ from stepped heating experiments (55). As a result, NWA 7034 is commonly used to infer the composition of an ancient water reservoir on Mars (59, 60); however, terrestrial contamination may have

Downloaded from https://www.pnas.org by 71.228.158.19 on April 25, 2025 from IP address 71.228.158.19.

Table 2. Mineral abundances determined by CheMin (amorphous-normalized)

Mineral*	MA†	±1σ	BD	±1σ	TC	±1σ	UB	±1σ
Plagioclase	31.2	4.1	21.2	0.9	15.2	1.7	14.8	2.3
K-feldspar	3.0	1.8	1.7	0.9	0.0	–	0.0	–
Pyroxene	5.2	3.5	3.5	2.0	8.7	1.9	6.0	1.6
Quartz	1.0	0.6	0.7	0.6	0.0	–	0.9	0.3
Magnetite	0.0	0	0.0	–	0.0	–	0.0	–
Hematite	0.9	1.6	8.4	1.1	0.0	–	2.3	1.4
Siderite	0.7	0.9	0.0	–	10.8	1.3	4.8	0.8
Ankerite	0.0	–	1.0	0.9	0.0	–	0.0	–
Anhydrite	1.9	1.3	0.8	0.7	0.8	0.6	0.5	0.4
Bassanite	0.2	0.2	2.5	0.7	1.5	0.9	0.8	0.2
Gypsum	0.0	–	0.2	0.4	0.0	–	2.3	0.3
Starkeyite	0.0	–	0.0	–	0.0	–	6.4	1.5
Kieserite	0.0	–	0.0	–	3.2	1.1	0.0	–
Phyllosilicate	28.7	10	12.0	6.0	0.0	–	0.0	–
Amorphous‡	27.0	20	45.0	12.5	60.1	11.5	60.0	
Opal-CT	0.0	–	3.0	–	0.0	–	0.0	–
TOTAL	99.8		100.0		100.0		98.8	

*Mineral abundances for each site are publicly available via the PDS (https://pds-geosciences.wustl.edu/missions/msl/chemin.html).
†This sample corresponds with the first sample at MA1. It will be referred to as MA for the remainder of the paper.
‡Amorphous mineral abundances are estimated via FullPAT analysis.

affected the lower $\delta^{18}O_{water}$ values (55). With this in mind, we will use the water isotopic composition of NWA 7034 as a comparison point for the oxygen isotope composition of the water(s) in equilibrium with the Gale crater carbonates.

Carbon isotope measurements at or below modern atmospheric CO_2 values were also obtained by pyrolysis of other Gale crater sediments by MSL. The evolved CO_2 isotopic compositions range from $\delta^{13}C = -24 \pm 44$ to 56 ± 11‰ and $\delta^{18}O = -36 \pm 59$ to 45 ± 10‰ (31). The CO_2 released during these experiments thermally evolved from a mixture of multiple endogenous and exogenous sources, adding to the complexity of the isotope data interpretation. Although some pyrolysis experiments released CO_2 at temperatures consistent with carbonates, these results correspond to scooped aeolian dune samples for which mineral provenance is essentially unknown. Given this geologic uncertainty, the large range in values, and the variety of mixed sources contributing to the CO_2 analyzed in the pyrolysis experiments of Franz et al. (31), we reserve further discussion of these putative carbonates in the Gale crater sediments for the cryogenic precipitation section below.

The remainder of the discussion will be dedicated to exploring mechanisms to explain the offset in $\delta^{13}C$ and $\delta^{18}O$ between the carbonates analyzed in this study and known martian volatile reservoirs (e.g., modern atmospheric CO_2, water in NWA 7034). While these reservoirs are not the actual sources of the carbonates, using modern atmospheric CO_2 and water in NWA 7034 as end-members requires the least amount of fractionation (among measured reservoirs) to achieve the isotopic enrichments measured in these carbonates. Therefore, the degree of heavy isotope enrichment in the carbonates relative to these end-members is likely a minimum estimate compared to the offset between the actual sources and the carbonates. We also investigate the range in $\delta^{13}C$ and $\delta^{18}O$ values between the samples as well as the notable span between $\delta^{13}C$ and $\delta^{18}O$ at MA, TC, and UB. The mechanisms discussed below are not mutually exclusive and in fact, achieving the observed heavy isotopic enrichments likely requires multiple mechanisms. While the main manuscript focuses on two preferred mechanisms, three more exotic mechanisms (cosmic ray ionizing radiation and spallation reactions, equilibration of CH_4 and CO with coexisting CO_2, and photochemistry involving ultraviolet radiation) are explored further within *SI Appendix, Supplemental Section*. These additional mechanisms are unusual on Earth but may be more relevant over long timescales on planets like Mars with thin atmospheres and an absence of biological activity.

Carbonate Precipitation. Carbonate minerals form through the precipitation of divalent metal cations and dissolved inorganic carbon (DIC) ions (e.g., H_2CO_3, HCO_3^-, and CO_3^{2-}), which result from the dissociation of carbonic acid derived from dissolution of CO_2 as shown in the following simplified reaction:

$$CO_2(aq) + H_2O(l) + M^{2+}(aq) \leftrightarrow MCO_3(s) + 2H^+(aq). \quad [1]$$

In this reaction, M is a divalent cation (e.g., Ca^{2+}, Mg^{2+}, and Fe^{2+}) that can be sourced from the weathering of silicate minerals or the dissolution of evaporite minerals. As rivers and lakes existed on early Mars (24), this is a viable mechanism to form the carbonates studied here. Aqueous carbonate precipitation is also consistent with the presence of bassanite ($CaSO_4 \cdot \frac{1}{2}H_2O$), gypsum ($CaSO_4 \cdot 2H_2O$), starkeyite ($MgSO_4 \cdot 4H_2O$), and kieserite ($MgSO_4 \cdot H_2O$) in varying proportions at the four drill sites (Table 2). While not necessarily contemporaneous with the carbonates, these hydrated sulfates indicate the past presence of liquid water at the same stratigraphic horizons, which is in turn consistent with sedimentological evidence for standing water in Gale crater (61).

The carbon and oxygen isotopic compositions of carbonate minerals precipitated from solution depend upon the carbon and oxygen isotopic composition of the DIC pool, the oxygen isotopic composition of the water, the temperature and pH of the system, and the rate and extent of reaction (62). Assuming

Downloaded from https://www.pnas.org by 71.228.158.19 on April 25, 2025 from IP address 71.228.158.19.

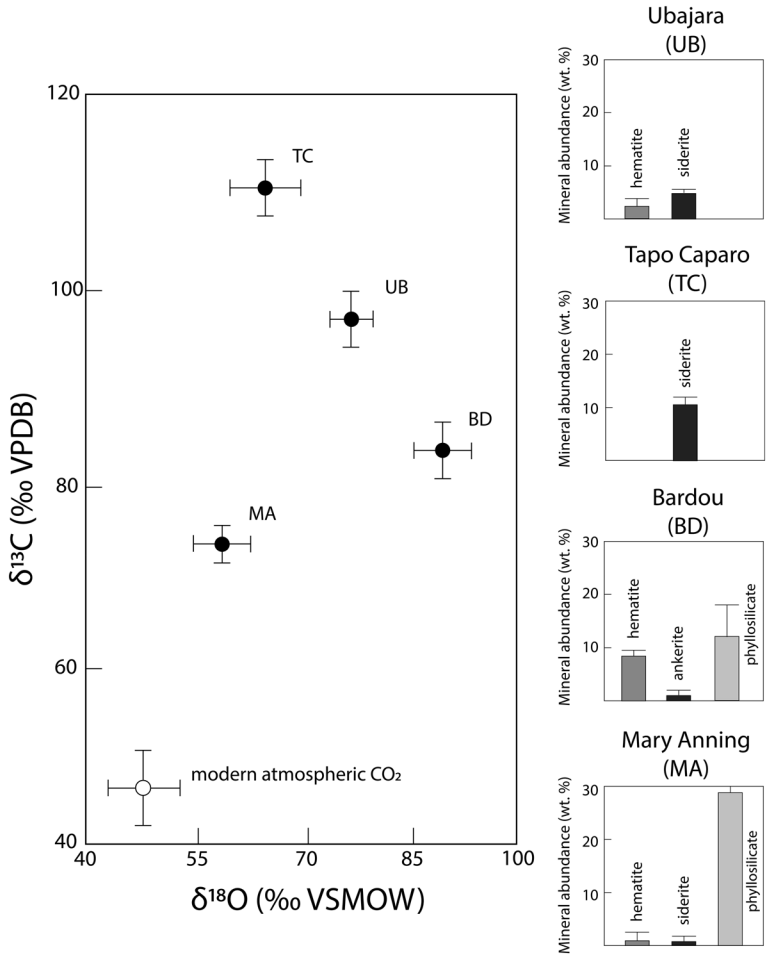

Fig. 2. Isotope and mineral data from four Gale crater carbonates. The large plot shows the carbon and oxygen isotope values of the carbonates (filled black circles) compared with modern atmospheric CO_2 (empty white circle) (35). The subplots illustrate the mineral abundances of carbonates, iron oxides, and phyllosilicates at each of the sites. Exact isotope and mineral abundance data can be found in Tables 1 and 2, respectively. Error bars correspond to 1 SE.

the carbonates formed in isotopic equilibrium with the aqueous system and were not subject to later isotopic exchange (e.g., diagenetic alteration and recrystallization), the $\delta^{13}C$ and $\delta^{18}O$ of the carbonates should preserve information regarding their formation conditions. In the case of the four samples presented here, such information aids in our understanding of the environmental conditions and processes present in Gale crater at the time of carbonate formation.

If the Gale crater carbonates formed in isotopic equilibrium in their respective settings, we would expect the $\delta^{13}C$ of the carbonates to reflect fractionation from the DIC pool (i.e., the CO_2 in reaction 1). Atmospheric loss has preferentially stripped ^{12}C from the atmosphere, progressively enriching the residual CO_2 in ^{13}C over time (43). Therefore, we expect that atmospheric CO_2 at the time of carbonate formation would have been depleted in ^{13}C relative to modern atmospheric CO_2 [$\delta^{13}C = 46 \pm 4‰$ (35)]. Modeling by Hu et al. (63) and Thomas et al. (64) supports this, suggesting that atmospheric CO_2 $\delta^{13}C$ values were ≤20‰ at the Hesperian-Amazonian boundary and ≤0‰ at the Noachian-Hesperian boundary. At 25 °C, $FeCO_3$ equilibrium with CO_2 produces a carbon isotope fractionation of $1000\ln^{13}\alpha_{\text{siderite-CO2}} = 8.5 \pm 0.2‰$ (65). Siderite precipitated at 25 °C in isotopic equilibrium with a DIC pool with $\delta^{13}C$ values of 0‰, 20‰, and 46‰ would have $\delta^{13}C$ values of 8.5‰, 28.5‰, and 54.5‰, respectively. Although this process produces ^{13}C-enriched carbonate, the $\delta^{13}C$ values of the Gale crater carbonates (≥72 ± 2‰, Fig. 3*A*) necessitate a DIC pool that is even more ^{13}C-enriched than the modern martian atmosphere. At temperatures approaching 0 °C, the magnitude of the siderite-CO_2 carbon isotope fractionation increases to >15‰ (65), which is still insufficient to account for the lowest carbonate $\delta^{13}C$ value (72 ± 2‰) reported here.

At equilibrium, the $\delta^{18}O$ of the carbonates is governed by that of the DIC pool, which itself is controlled by oxygen isotopic exchange with water. Water in isotopic equilibrium with atmospheric CO_2 has a $\delta^{18}O$ value approximately 40‰ lower than that of the corresponding CO_2 (69). A standing body of water that was in oxygen isotopic equilibrium with modern martian atmospheric CO_2 in the Gale crater should have a $\delta^{18}O$ value of 8‰. Theoretical modeling by Chacko & Deines (66) predicts that the oxygen isotope fractionation between siderite ($FeCO_3$) and water should be $1000\ln^{18}\alpha_{\text{siderite-H2O}} = 30.03‰$ at 25 °C, enriching the $FeCO_3$ in ^{18}O relative to H_2O. The corresponding fractionation factor between ankerite ($Ca[Fe,Mg,Mn][CO_3]_2$) and water is slightly lower at $1000\ln^{18}\alpha_{\text{ankerite-H2O}} = 28.52‰$. More ^{18}O is partitioned into the carbonate as temperature decreases; at 0 °C, the corresponding fractionation factors between carbonate are $1000\ln^{18}\alpha_{\text{siderite-H2O}} = 35.61‰$ and $1000\ln^{18}\alpha_{\text{ankerite-H2O}} = 33.93‰$. The magnitude of the equilibrium isotope fractionation between water with a $\delta^{18}O$ value of ~8‰ and either of the carbonates is insufficient to explain the $\delta^{18}O$ values of the Gale crater carbonates.

Based on these preceding $1000\ln\alpha$ values, waters in isotopic equilibrium with the Gale crater carbonates would need to have $\delta^{18}O$ values between 23 to 57‰ at 0 °C and 29 to 63‰ at 25 °C (Fig. 3*B*). As of this writing, there are no known measurements of ancient Martian water this enriched in ^{18}O. Stepwise heating of

Downloaded from https://www.pnas.org by 71.228.158.19 on April 25, 2025 from IP address 71.228.158.19.

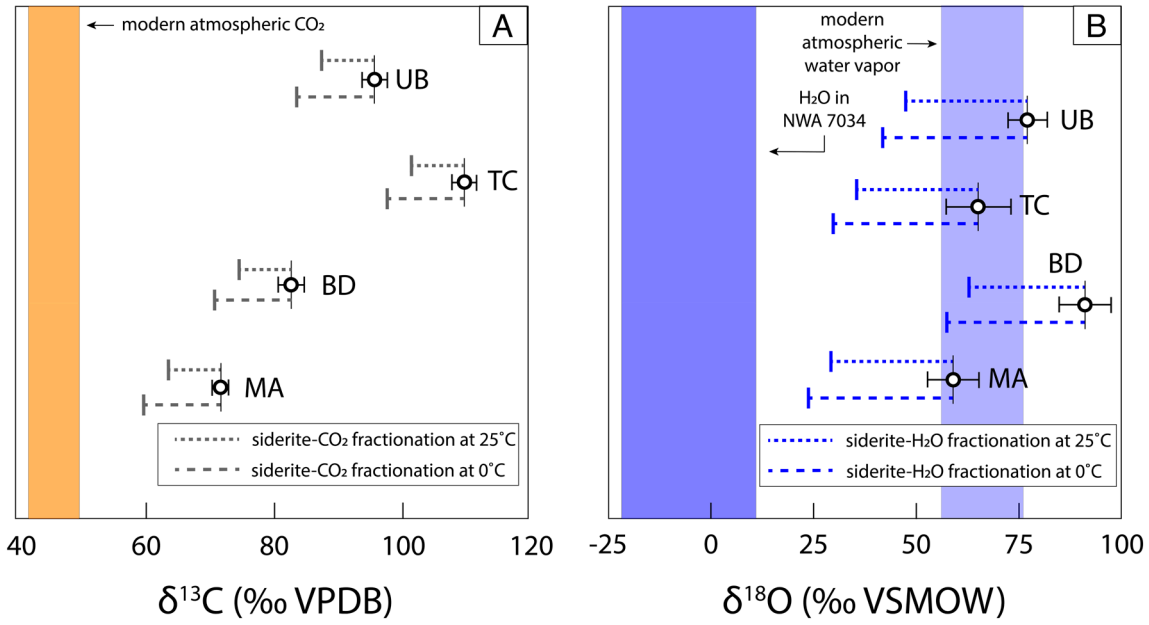

Fig. 3. (*A*) Carbon and (*B*) oxygen isotope data from carbonates identified by the Curiosity rover within Gale crater. The dotted and dashed lines illustrate the equilibrium isotope fractionations at 25 °C and 0 °C, respectively, between the carbonate and the relevant source material (CO_2 for carbon isotopes and H_2O for oxygen isotopes) (65–68). The orange box in *A* represents modern atmospheric CO_2 (35) while the light and dark blue boxes in *B* represent modern atmospheric water vapor and water from stepped heating of Martian meteorite NWA 7034 (55). None of these reservoirs were present when the Gale crater carbonates formed; however, they provide valuable context for the relative enrichment in ^{13}C and ^{18}O of the carbonates. Error bars correspond to 1 SE in both panels.

Martian meteorite NWA 7034 from 50-1,000 °C produced $\delta^{18}O_{water}$ values from −21.78 ± 0.05‰ to 11.02 ± 0.04‰ (55). The corresponding bulk $\delta^{18}O$ values of NWA 7034 are also the highest among the SNC meteorites (55). However, if the water in Gale was as isotopically enriched as the most ^{18}O-enriched water from NWA 7034, any carbonates precipitating in isotopic equilibrium with those fluids would only have a $\delta^{18}O$ value of ~46‰, far below those measured in the Gale crater carbonates (Fig. 4).

Two recent papers presented measurements of modern atmospheric water vapor on Mars: 1) SAM analyses in Gale crater provided atmospheric $\delta^{18}O_{water}$ values of 84 ± 10‰ (35), and 2) infrared measurements from the ExoMars Trace Gas Orbiter placed the $\delta^{18}O_{water}$ value of atmospheric water vapor at 200 ± 80‰ (71).

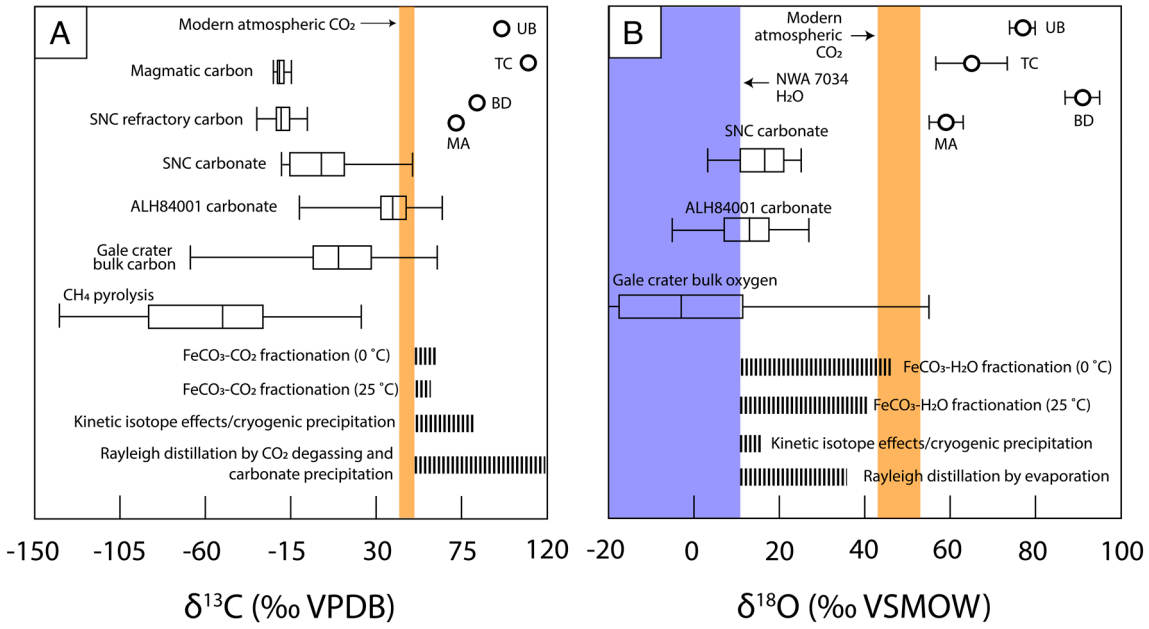

Fig. 4. Measured (*A*) carbon and (*B*) oxygen isotope values from the four Gale crater carbonates compared with different carbon and oxygen reservoirs in Martian materials. These materials include magmatic carbon (48), SNC refractory carbon (70), SNC carbonates (1, 50), ALH84001 carbonates (12, 50, 57), bulk carbon and oxygen (2, 31), and CH_4 from pyrolysis of mixed carbon components in sediments (3). The orange boxes in each subplot represent the range of values for modern atmospheric CO_2 (35), which places an upper limit on inferred ancient atmospheric CO_2. The blue box in *B* represents the range of $\delta^{18}O$ values measured in water evolved from SNC meteorite NWA 7034 during stepped heating experiments (55). Dashed boxes illustrate the maximum potential isotopic fractionation generated by each respective process assuming that the volatile phase in each has an isotopic composition corresponding to that of the CO_2 or H_2O reservoir. Error bars in panel (*B*) correspond to 1 SE; the error bars in panel (*A*) are smaller than the data points.

Downloaded from https://www.pnas.org by 71.228.158.19 on April 25, 2025 from IP address 71.228.158.19.

The $\delta^{18}O$ value determined by Webster et al. (35) represents water evolved from scooped aeolian fines at Rocknest (RN3). Although initially interpreted as adsorbed atmospheric water vapor, a reassessment of the RN3 cut analyzed by the TLS indicates that the evolved water is a mixture of adsorbed water and water evolved from hydrated salts including chlorides, sulfates, and oxyhydroxides. Therefore, this value cannot be considered entirely representative of modern atmospheric water vapor. The ExoMars data must also be placed into context as they were integrated across multiple altitudes and times to give a weighted $\delta^{18}O$ value for the Martian atmosphere. Notably, the lowest altitude accessible by these measurements is 15 km above the surface, meaning that the 200 ± 80‰ value does not necessarily represent the same portion of the atmosphere measured by SAM. Given the higher altitudes, the sections of the atmosphere measured by ExoMars may be subject to greater degrees of photochemical alteration and loss than the surface atmosphere, which would accentuate any isotopic fractionation in the upper atmosphere (72). In addition, both the SAM and ExoMars results are measurements of water vapor rather than liquid water. At 0 °C, the $1000\ln^{18}\alpha_{H2O(l)\text{-}H2O(g)}$ = 11.77‰ (73), meaning that any liquid water in equilibrium with those water vapor reservoirs would be even further from the carbonate $\delta^{18}O$ values. While none of these $\delta^{18}O_{water}$ measurements overlap with the range of theoretical $\delta^{18}O_{water}$ values needed to generate the carbonates, this does not rule out the possibility that such waters existed either as an unmixed reservoir or as the mixing product of an ^{18}O-depleted reservoir (e.g., the water in NWA 7034) and an ^{18}O-enriched reservoir (e.g., modern measurements from SAM and ExoMars). Given that such reservoirs are inherently heterogeneous, we will consider alternative pathways capable of producing the ^{13}C and ^{18}O enrichments measured in these carbonates.

Evaporation and Rayleigh Fractionation. In the preceding section, we determined that the Gale crater carbonates could not have formed in isotopic equilibrium with a DIC pool and water that had carbon and oxygen isotopic compositions equal to those in known Martian materials. It is, however, possible that the Gale crater carbonates formed in isotopic equilibrium with water and DIC enriched in ^{13}C and ^{18}O. Rayleigh-type processes, such as evaporation, can amplify isotopic fractionation during progressive loss of the lighter isotopes from the liquid in an open or partially open system, leaving the residual water enriched in heavy isotopes relative to the original fluid (74–76). Multiple lines of geologic and geochemical evidence indicate that water levels in the Gale crater have fluctuated over time (9, 77, 78). Progressive water loss through evaporation, with associated carbonate precipitation and CO_2 exsolution, would drive both the $\delta^{18}O_{water}$ and the $\delta^{13}C$ of the DIC to higher values relative to the initial fluid, as has been demonstrated in evaporative models for Earth (79) and Martian meteorites (80). At equilibrium, the oxygen isotopic fractionation between liquid water and water vapor is governed by the following equation:

$$1000\ln^{18}\alpha_{H2O(l)-H2O(g)} = -7.685 + 6.7123\left(10^3/T\right) - 1.6664\left(10^6/T^2\right) + 0.35041\left(10^9/T^3\right), \quad [2]$$

where temperature is measured in kelvin (73). At 0 °C, this empirical relationship predicts that liquid water will be enriched in ^{18}O by 11.8‰ relative to the water vapor. A similar relationship exists for the carbon isotopic composition of the DIC pool. Previous work by Zhang et al. (81) established the following fractionations between DIC species and gaseous CO_2 produced by exsolution:

$$1000\ln^{13}\alpha_{HCO3-CO2} = -0.141(T) + 10.78, \quad [3]$$

$$1000\ln^{13}\alpha_{CO3-CO2} = -0.052(T) + 7.22, \quad [4]$$

$$1000\ln^{13}\alpha_{CO2(aq)-CO2(g)} = -0.0049(T) - 1.31, \quad [5]$$

where the temperatures are measured in kelvin. These equations predict ^{13}C enrichment in the dissolved carbonate and bicarbonate ions relative to the gaseous CO_2 at temperatures that support liquid water. Importantly, these carbon and oxygen isotope fractionations will establish the isotopic compositions of the water and DIC pool from which the carbonates are precipitating. By themselves, the fractionations in Eqs. 2–5 and the associated siderite–water fractionation [$1000\ln^{18}\alpha_{siderite\text{-}H2O}$ = 30.03‰ at 25 °C (66)] and siderite–CO_2 fractionation [$1000\ln^{13}\alpha_{siderite\text{-}CO2}$ = 8.5 ± 0.2‰ at 25 °C (65)] are not sufficient to reproduce the $\delta^{13}C$ and $\delta^{18}O$ values of the Gale crater carbonates. However, as mentioned above, the $\delta^{13}C$ and $\delta^{18}O$ of the water and DIC pool can be increased by evaporative processes.

The conditions required for such fractionation might occur within a shallow subsurface setting that is no longer in contact with the atmosphere. In their water–rock model for meteorite ALH84001, Halevy et al. (80) hypothesized that a sufficient degree of evaporation (≥90%) could generate changes in $\delta^{13}C$ and $\delta^{18}O$ as large as 40‰ and 25‰, respectively. This degree of evaporation, when combined with the equilibrium fractionation factors for carbon [$1000\ln^{13}\alpha_{siderite\text{-}CO2}$ = 8.5 ± 0.2‰ at 25 °C (65) and oxygen [$1000\ln^{18}\alpha_{siderite\text{-}H2O}$ = 35.61‰ at 0 °C (66) isotopes, would require starting compositions of $\delta^{13}C_{CO2}$ = 23 to 61‰ and $\delta^{18}O_{H2O}$ = −2 to 30‰ in order to produce the $\delta^{13}C$ and $\delta^{18}O$ values of the Gale crater carbonates. While this combination of equilibrium fractionation and evaporation can entirely explain only two of the isotope enrichments (MA $\delta^{18}O$ = 59 ± 4‰; TC $\delta^{18}O$ = 65 ± 5‰), it is possible that the larger enrichments in ^{13}C and ^{18}O measured in the Gale carbonates are simply a function of carbonate precipitation from an aqueous system that has experienced greater degrees of evaporation than that hypothesized for the much older carbonates entrained in ALH84001.

The evaporative interpretation also matches well with the sedimentary context and mineralogy of the four samples (Fig. 2 and Table 2). The mudstones identified at MA point toward a lacustrine origin while the sandstones at BD indicate a marginal lake environment (Fig. 1). TC and UB both overlie a relatively resistant unit in the Catrimani Member known as the Marker Band (82) (Fig. 1) and the mixture of scours and low-angle cross-bedding at the two sites has been interpreted as aeolian. TC and UB, the sites with the highest carbonate abundances (10.8 wt.% and 4.8 wt.% siderite, respectively) and highest $\delta^{13}C$ values, are located within the sulfate unit, while MA and BD were sampled in the clay mineral-rich Glen Torridon region and the clay-sulfate transition zone, respectively. These latter two samples contain significantly less carbonate: MA has the lowest amount of siderite (1.4 wt.%), while BD contains carbonate as ankerite (1.0 wt.%).

The range of formation environments (lacustrine, marginal, and aeolian) is consistent with the idea that these samples experienced differing degrees of hydration and, by extension, evaporation. Within this framework, the lower $\delta^{13}C$ and $\delta^{18}O$ values at MA could be a function of equilibrium fractionation and evaporation within a shallow lake while the elevated $\delta^{13}C$ and $\delta^{18}O$ values at BD, TC, and UB might be the result of more extensive evaporation in periodically or occasionally submerged settings (i.e., lake margins, sabkhas). These types of alternating wet–dry

Downloaded from https://www.pnas.org by 71.228.158.19 on April 25, 2025 from IP address 71.228.158.19.

settings have been previously proposed based on deposits identified in between BD and TC (77). Furthermore, this interpretation is consistent with one of the leading hypotheses for the formation of the Marker Band: precipitation of indurated sulfates in a lacustrine environment (83, 84).

It is also possible that these wet–dry cycles resulted in secondary diagenetic events that contributed to the range of $\delta^{18}O$ values and carbonate abundances. The presence of hematite (8.4 wt.% and 0.9 wt.%) and phyllosilicates (12.0 wt.% and 28.7 wt.%) at BD and MA suggests that there may have been fluid-induced diagenesis within the clay-sulfate unit, possibly during a later, more extensive diagenetic event. Diagenesis might also explain the lower concentrations of carbonate at BD and MA as this mechanism was previously proposed by Thorpe et al. (11) to explain a spatial transition from smectites to Fe-carbonates to hematite as the result of proximity to a mixing zone. Another possibility is that the $\delta^{18}O$ value of TC (65 ± 5‰) reflects recrystallization in a solution with a different $\delta^{18}O$ from the original carbonate source(s). Carbonate recrystallization on Earth can affect both $\delta^{13}C$ and $\delta^{18}O$ (85); however, changes in $\delta^{13}C$ require fluids with high DIC concentration, which have not been observed on Mars. Recrystallization in a DIC-poor fluid could therefore lower $\delta^{18}O$ while not affecting $\delta^{13}C$, offering an explanation for why TC does not seem to follow the same evaporative trend in $\delta^{13}C$ and $\delta^{18}O$ that the other three sites exhibit (Fig. 2). A more detailed analysis of the distribution of soluble cations within different mineral phases could provide further evidence for these hypotheses.

Cryogenic Brine Precipitation. Cryogenic precipitation (T ≈ 0 °C) is a compelling explanation for the observed isotope values as it has previously been demonstrated to produce ^{13}C and ^{18}O enrichments in carbonates (86–88), and cold temperatures are consistent with some models of early Mars climate (31). While liquid water once existed on Mars (89), it is not known when these bodies of water transitioned from long-lasting to more ephemeral surface features (78). Given this uncertainty, we do not know whether the carbonates precipitated under warm (90) (≥25 °C) or cryogenic conditions (91). Cryogenic carbonates have been identified on Earth, including in permafrost caves (86) and aufeis deposits (92). In both settings, freezing concentrates solutes within bicarbonate-rich waters, driving CO_2 degassing, pH rise, and precipitation of carbonates and other salts. Freezing processes such as these have been theorized to have occurred on Mars (93). Such cryobrines can form not only carbonates but also hydrated sulfate minerals (93) like those that have been detected at BD, MA, TC, and UB (Table 2). Moreover, as in a purely evaporative scenario, CO_2 exsolving from these fluids would remove ^{12}C and ^{16}O, leaving the water and DIC from which the carbonates precipitate relatively enriched in ^{13}C and ^{18}O.

Precipitation under cryogenic conditions also introduces the potential for kinetic isotope effects (KIE) as the lower temperatures would reduce the rates of isotopic exchange. Under isotopic equilibrium at ~25 °C, experiments show that the fractionations between siderite and CO_2 are $1000\ln^{13}\alpha_{siderite\text{-}CO2} = 8.5 \pm 0.2‰$ (65) and $1000\ln^{18}\alpha_{siderite\text{-}CO2} = -8.09‰$ (94). In other words, ^{18}O will preferentially fractionate into the CO_2 rather than siderite at 25 °C. Crucially, these fractionation factors assume equilibrium between the siderite and CO_2. This assumption is not necessarily reasonable in a setting like the Martian surface where low temperatures and high salinities may amplify kinetic effects (57), yielding fractionations that diverge from those predicted by equilibrium fractionation factors. Clark and Lauriol (86) examined these KIE in natural and synthetic cryogenic carbonates. They found that at 0 °C, the $\delta^{13}C$ value of carbonate was 31.2 ± 1.5‰ higher than that of the dissolved CO_2. This is three times greater than the predicted $CaCO_3$-CO_2 equilibrium fractionation (10.3‰). The corresponding kinetic $1000\ln^{18}\alpha_{calcite\text{-}CO2}$ for $\delta^{18}O$ is lower (5.5 ± 0.5‰) but favors ^{18}O-enrichment in the carbonate. As surface temperatures on early Mars may have regularly dropped below 0 °C, similar KIE fractionations may occur during cryogenic precipitation of siderite and ankerite on Mars. These fractionations, where ^{13}C partitioning is stronger than ^{18}O by ~25‰, provide a mechanism for the additional enrichment in $\delta^{13}C$ measured at TC and UB. However, the magnitude of the variation between the ^{13}C and ^{18}O fractionations is smaller than the difference between the $\delta^{13}C$ and $\delta^{18}O$ values, which exceeds 40‰ at TC. A possible scenario is that CO_2 exsolution and/or evaporation during cryogenic brine precipitation yielded the fractionation necessary to produce the carbonate $\delta^{13}C$ values from atmospheric CO_2, although neither evaporation nor cryogenic brine precipitation can produce the enhanced ^{18}O enrichment (relative to ^{13}C) at BD. Therefore, while KIEs associated with rapid mineral precipitation remain a possible explanation, the simplest and most probable mechanism for generating the observed $\delta^{13}C$ and $\delta^{18}O$ values is a combination of evaporation, CO_2 exsolution, and the associated equilibrium isotope fractionations.

Conclusions

We discuss Fe-carbonates detected at four locations within the Gale crater. The carbon ($\delta^{13}C$ = 72 ± 2 to 110 ± 3‰ VPDB) and oxygen ($\delta^{18}O$ = 59 ± 4 to 91 ± 4‰ VSMOW) isotope values of these carbonates are highly enriched in heavy isotopes relative to all known samples from Mars, motivating an investigation of their origin(s). This study explores two probable mechanisms for generating these enrichments: 1) equilibrium isotopic fractionation between carbonates and a DIC-bearing aqueous solution that has been isotopically enriched in ^{13}C and ^{18}O due to evaporative water loss and associated CO_2 exsolution and 2) KIEs associated with cryogenic brine precipitation. However, none of these mechanisms alone completely explains the isotopic compositions of all four carbonates. It is probable that a combination of these processes is responsible for the isotopic enrichments. One potential scenario is that the carbonates formed via Rayleigh-type evaporative processes and CO_2 exsolution induced by intermittent wet–dry cycles within Gale crater. The differences in isotopic values between the sites can be attributed to the carbonates having precipitated from fluids that experienced different degrees of evaporative water loss with concomitant CO_2 exsolution. This explanation matches the mineralogy for the four sites, where BD and MA have a suite of clay minerals associated with lacustrine environments while TC and UB match the features of aeolian deposits. Further mineralogical analysis, modeling of isotopic evolution (80), and analog experiments would provide additional means of testing this hypothesis.

Materials and Methods

The 5-km tall sedimentary mound in the center of the Gale crater known as Mt. Sharp preserves a complex sedimentary history and likely records a transition in Mars' ancient climate (25). The mineralogical data from CheMin play a key part in unraveling that history. The first drill hole in the Yellowknife Bay formation revealed abundant clay minerals in most fluvial-lacustrine sedimentary rocks (61, 95, 96). However, in the last three years, continued exploration of the crater has uncovered a transition in the stratigraphy as well as the mineralogy. The sedimentology of outcrops farther up in the Carolyn Shoemaker formation documents a shift from fluvial and lacustrine environments to terrains that were dominated by aeolian processes. This

Downloaded from https://www.pnas.org by 71.228.158.19 on April 25, 2025 from IP address 71.228.158.19.

shift in the stratigraphy coincides with an overall loss of clay minerals and an increase in sulfates and carbonates (32).

CheMin. The CheMin X-ray diffractometer measures the mineralogy of scooped soils and drilled rock samples (97). Drill powders are delivered to the CheMin instrument and funneled into sample cells with Mylar or Kapton windows. A piezoelectric actuator vibrates the sample cell to promote randomization of the particles as the X-ray beam passes through with a transmission geometry. As X-rays diffract from the interaction with mineral phases, diffraction patterns are collected as two-dimensional images on a charge-coupled device and then are converted to one-dimensional patterns using a modified version of the GSE_ADA software (98). The data are analyzed with whole pattern fitting FULLPAT (99, 100) and Rietveld refinement methods to 1) estimate the proportions of crystalline, clay mineral, and amorphous components, 2) identify crystalline phases present at >1 wt%, and 3) measure unit-cell parameters for major crystalline phases.

SAM. The samples discussed in this study were acquired from fluvial–lacustrine and aeolian deposits across a ~400 m change in elevation during the ascent of Aeolis Mons. Data presented here were acquired using SAM's TLS instrument (36). Drilled samples are prepared using feed-extended sample transfer, whereby sample fines are stored within the drill stem and then vibrated and rotated prior to delivery into SAM (37). The sample was delivered to SAM's solid sample inlet into a preconditioned quartz glass cup (heated to ~870 °C and cooled before sample delivery) and sealed into one of two SAM ovens. Samples were heated at ~35 °C/min to ~870 °C under helium flow (~0.8 sccm). Additional details of evolved gas quantification, including estimation of delivered sample mass and analysis by the quadrupole mass spectrometer, have been described elsewhere (101, 102). In each experiment, a portion of gas evolved over a previously determined temperature interval (typically ~100 to 300 °C wide) was sent to the SAM TLS for isotopic analysis of CO_2 and water (*SI Appendix*, Figs. S1–S4). The TLS is described in detail elsewhere (103).

Data, Materials, and Software Availability. Flight mass spectrometry and tunable laser spectrometry data have been deposited in the Geosciences Node of NASA's Planetary Data System (https://pds-geosciences.wustl.edu/missions/msl/sam.htm) (104). All study data are included in the article and/or *SI Appendix*.

ACKNOWLEDGMENTS. This research could not have been completed without the dedication and hard work of the MSL team. We would like to additionally thank the SAM and CheMin science and operations teams for their contributions. This work benefitted from thorough reviews from Ethan Grossman and an anonymous reviewer as well as helpful discussions with John Grotzinger and Richard Becker. The Jet Propulsion Laboratory is operated by the California Institute of Technology under contract with the NASA (80NM0018D0004). Finally, D.G.B.'s research was supported by an appointment to the NASA Postdoctoral Program at the NASA Goddard Space Flight Center facility, administered by Oak Ridge Associated Universities under contract with NASA.

Author affiliations: [a]NASA Postdoctoral Fellow, Solar System Exploration Division, NASA Goddard Space Flight Center, Greenbelt, MD 20771; [b]Solar System Exploration Division, NASA Goddard Space Flight Center, Greenbelt, MD 20771; [c]NASA Jet Propulsion Laboratory, California Institute of Technology, Pasadena, CA 91109; [d]Jacobs Technology, Houston, TX 77058; [e]NASA Johnson Space Center, Houston, TX 77058; [f]University of Maryland/Goddard Space Flight/Center for Research and Exploration in Space and Science Technology (CRESST II), Greenbelt, MD 20771; [g]Department of Geophysical Sciences, University of Chicago, Chicago, IL 60637; [h]Department of Geosciences, Pennsylvania State University, University Park, PA 16802; [i]Department of Geoscience, University of Calgary, Calgary, AB T2N 1N4, Canada; and [j]NASA Ames Research Center, Moffett Field, CA 94043

Author contributions: D.G.B., J.C.S., C.R.W., H.B.F., B.S., M.T.T., C.H.H., A.C.M., and C.A.M. designed research; D.G.B., J.C.S., C.R.W., H.B.F., B.S., M.T.T., C.H.H., A.C.M., and C.A.M. performed research; D.G.B., J.C.S., C.R.W., H.B.F., M.T.T., E.S.K., J.L.E., A.A.P., C.H.H., and E.B.R. analyzed data; and D.G.B., J.C.S., C.R.W., A.E.H., H.B.F., B.S., M.T.T., E.S.K., J.L.E., A.A.P., C.H.H., B.M.T., D.J.D.M., E.B.R., and A.C.M. wrote the paper.

1. M. M. Grady, I. Wright, The carbon cycle on early Earth–and on Mars? *Phil. Trans. R. Soc. Lond. Biol. B Sci.* **361**, 1703–1713 (2006).
2. J. C. Stern *et al.*, Organic carbon concentrations in 3.5-billion-year-old lacustrine mudstones of Mars. *Proc. Natl. Acad. Sci. U.S.A.* **119**, 1–8 (2022).
3. C. H. House *et al.*, Depleted carbon isotope compositions observed at Gale crater, Mars. *Proc. Natl. Acad. Sci. U.S.A.* **119**, 1–10 (2022).
4. J. L. Bandfield, T. D. Glotch, P. R. Christensen, Spectroscopic identification of carbonate minerals in the Martian dust. *Science* **301**, 1084–1087 (2003).
5. B. L. Ehlmann *et al.*, Orbital identification of carbonate-bearing rocks on Mars. *Science* **322**, 1828–1832 (2008).
6. W. V. Boynton *et al.*, Evidence for calcium carbonate at the Mars Phoenix landing site. *Science* **325**, 61–64 (2009).
7. R. V. Morris *et al.*, Identification of carbonate-rich outcrops on mars by the spirit rover. *Science* **421**, 1–5 (2010).
8. J. R. Michalski, P. B. Niles, Deep crustal carbonate rocks exposed by meteor impact on Mars. *Nat. Geosci.* **3**, 751–755 (2010).
9. P. B. Niles *et al.*, Geochemistry of carbonates on Mars: Implications for climate history and nature of aqueous environments. *Space Sci. Rev.* **174**, 301–328 (2013).
10. A. M. Zastrow, T. D. Glotch, Distinct carbonate lithologies in Jezero Crater, Mars. *Geophys. Res. Lett.* **48**, 1–10 (2021).
11. M. T. Thorpe *et al.*, Mars Science Laboratory CheMin data from the glen torridon region and the significance of lake-groundwater interactions in interpreting mineralogy and sedimentary history. *J. Geophys. Res. Planets* **127**, e2021JE007099 (2022).
12. C. S. Romanek *et al.*, Record of fluid-rock interactions on Mars from the meteorite ALH84001. *Nature* **372**, 655–657 (1994).
13. J. C. Bridges *et al.*, Alteration assemblages in Martian meteorites: Implications for nearsurface processes. *Space Sci. Rev.* **96**, 365–392 (2001).
14. J. M. Eiler, J. W. Valley, C. M. Graham, J. Fournelle, Two populations of carbonate in ALH84001: Geochemical evidence for discrimination and genesis. *Geochim. Cosmochim. Acta* **66**, 1285–1303 (2002).
15. A. H. Treiman, The nakhlite meteorites: Augite-rich igneous rocks from Mars. *Geochemistry* **65**, 203–270 (2005).
16. J. C. Bridges, L. J. Hicks, A. H. Treiman, "Carbonates on Mars" in *Volatiles in the Martian Crust*, J. Filiberto, S. Schwenzer, Eds. (Elsevier, 2019), pp. 89–118.
17. E. L. Scheller *et al.*, Formation of magnesium carbonates on earth and implications for Mars. *J. Geophys. Res. Planets* **126**, 1–32 (2021).
18. B. H. N. Horgan, R. B. Anderson, G. Dromart, E. S. Amador, M. S. Rice, The mineral diversity of Jezero crater: Evidence for possible lacustrine carbonates on Mars. *Icarus* **339**, 113526 (2020).
19. A. J. Brown *et al.*, Hydrothermal formation of Clay-Carbonate alteration assemblages in the Nili Fossae region of Mars. *Earth Planet. Sci. Lett.* **297**, 174–182 (2010).
20. S.-T. Kim, J. R. O'Neil, Equilibrium and nonequilibrium oxygen isotope effects in synthetic carbonates. *Geochim. Cosmochim. Acta* **61**, 3461–3475 (1997).
21. E. L. Grossman, "Oxygen isotope stratigraphy" in *The Geologic Time Scale 2012*, F. Gradstein, J. Ogg, M. Schmitz, G. Ogg, Eds. (Elsevier, 2012), pp. 181–206.
22. G. L. Foster, J. W. B. Rae, Reconstructing ocean pH with boron isotopes in foraminifera. *Annu. Rev. Earth Planet. Sci.* **44**, 207–237 (2016).
23. D. L. Royer, R. A. Berner, D. J. Beerling, Phanerozoic atmospheric CO_2 change: Evaluating geochemical and paleobiological approaches. *Earth Sci. Rev.* **54**, 349–392 (2001).
24. E. S. Kite, Geologic constraints on early Mars climate. *Space Sci. Rev.* **215** (2019).
25. R. E. Milliken, J. P. Grotzinger, B. J. Thomson, Paleoclimate of Mars as captured by the stratigraphic record in Gale Crater. *Geophys. Res. Lett.* **37**, 1–6 (2010).
26. B. J. Thomson *et al.*, Constraints on the origin and evolution of the layered mound in Gale Crater, Mars using Mars Reconnaissance Orbiter data. *Icarus* **214**, 413–432 (2011).
27. L. L. Deit *et al.*, Sequence of infilling events in gale crater, mars: Results from morphology, stratigraphy, and mineralogy. *J. Geophys. Res. Planets* **118**, 2439–2473 (2013).
28. A. A. Fraeman *et al.*, The stratigraphy and evolution of lower Mount Sharp from spectral, morphological, and thermophysical orbital data sets. *J. Geophys. Res. Planets* **121**, 1713–1736 (2016).
29. B. Bultel, J. Viennet, F. Poulet, J. Carter, S. C. Werner, Detection of carbonates in Martian weathering profiles. *J. Geophys. Res. Planets* **124**, 989–1007 (2019).
30. T. F. Bristow *et al.*, Low Hesperian P_{CO2} constrained from in situ mineralogical analysis at Gale Crater, Mars. *Proc. Natl. Acad. Sci. U.S.A.* **114**, 2166–2170 (2017).
31. H. B. Franz *et al.*, Indigenous and exogenous organics and surface–atmosphere cycling inferred from carbon and oxygen isotopes at Gale crater. *Nat. Astronomy* **4**, 526–532 (2020).
32. E. B. Rampe *et al.*, "Mineralogical trends over the clay-sulfate transition in Gale crater from the Mars Science Laboratory CheMin instrument" in *53rd Lunar and Planetary Science Conference* (Lunar and Planetary Institute, The Woodlands, TX, 2022).
33. B. C. Gill, T. W. Lyons, T. D. Frank, Behavior of carbonate-associated sulfate during meteoric diagenesis and implications for the sulfur isotope paleoproxy. *Geochim. Cosmochim. Acta* **72**, 4699–4711 (2008).
34. T. F. Bristow *et al.*, Brine-driven destruction of clay minerals in Gale crater, Mars. *Science* **373**, 198–204 (2021).
35. C. R. Webster *et al.*, Isotope ratios of H, C, and O in CO_2 and H_2O of the Martian atmosphere. *Science* **341**, 260–264 (2013).
36. P. R. Mahaffy *et al.*, The sample analysis at mars investigation and instrument suite. *Space Sci. Rev.* **170**, 401–478 (2012).
37. A. C. McAdam *et al.*, Evolved gas analyses of sedimentary rocks from the glen torridon clay-bearing unit, Gale Crater, Mars: Results From the Mars Science Laboratory sample analysis at Mars instrument suite. *J. Geophys. Res. Planets* **127**, e2022JE007179 (2022).
38. J. M. T. Lewis *et al.*, Pyrolysis of oxalate, acetate, and perchlorate mixtures and the implications for organic salts on Mars. *J. Geophys. Res. Planets* **126**, e2020JE006803 (2021).
39. P. R. Mahaffy *et al.*, Abundance and isotopic composition of gases in the Martian atmosphere from the curiosity rover. *Science* **341**, 263–266 (2013).
40. C. R. Webster *et al.*, Mars methane detection and variability at Gale crater. *Science* **347**, 415–417 (2015).
41. H. Graven, R. F. Keeling, J. Rogelj, Changes to carbon isotopes in atmospheric CO_2 over the industrial era and into the future. *Global Biogeochem. Cycles* **34**, e2019GB006170 (2020).
42. M. H. Thiemens, S. Chakraborty, T. L. Jackson, Decadal $\Delta 17O$ record of tropospheric CO_2: Verification of a stratospheric component in the troposphere. *J. Geophys. Res. Atmos.* **119**, 6221–6229 (2014).
43. B. M. Jakosky, J. H. Jones, The history of Martian volatiles. *Rev. Geophys.* **35**, 1–16 (1997).
44. J. Alday *et al.*, Isotopic composition of CO_2 in the atmosphere of Mars: Fractionation by diffusive separation observed by the exomars trace gas orbiter. *J. Geophys. Res. Planets* **126**, e2021JE006992 (2021).

Downloaded from https://www.pnas.org by 71.228.158.19 on April 25, 2025 from IP address 71.228.158.19.

45. Y. Ueno *et al.*, Synthesis of ^{13}C-depleted organic matter from CO in a reducing early Martian atmosphere. *Nat. Geosci.* **17**, 503–507 (2024).
46. R. Wordsworth *et al.*, Transient reducing greenhouse warming on early Mars. *Geophys. Res. Lett.* **44**, 665–671 (2017).
47. T. A. Livengood *et al.*, Evidence for diurnally varying enrichment of heavy oxygen in Mars atmosphere. *Icarus* **335**, 113387 (2020).
48. M. M. Grady, A. B. Verchovsky, I. P. Wright, Magmatic carbon in Martian meteorites: Attempts to constrain the carbon cycle on Mars. *Int. J. Astrobiol.* **3**, 117–124 (2004).
49. A. Steele *et al.*, A reduced organic carbon component in martian basalts. *Science* **337**, 212–215 (2012).
50. A. J. T. Jull, C. J. Eastoe, S. Cloudt, Isotopic composition of carbonates in the SNC meteorites, Allan Hills 84001 and Zagami. *J. Geophys. Res. Planets* **102**, 1663–1669 (1997).
51. A. J. T. Jull, C. J. Eastoe, S. Xue, G. F. Herzog, Isotopic composition of carbonates in the SNC meteorites Allan Hills 84001 and Nakhla. *Meteoritics* **30**, 311–318 (1995).
52. L. Borg, M. J. Drake, A review of meteorite evidence for the timing of magmatism and of surface or near-surface liquid water on Mars. *J. Geophys. Res. Planets* **110**, 1–10 (2005).
53. J. P. Grotzinger *et al.*, Deposition, exhumation, and paleoclimate of an ancient lake deposit, Gale crater, Mars. *Science* **350**, aac7575 (2015).
54. P. E. Martin *et al.*, Billion-year exposure ages in Gale crater (Mars) indicate Mount Sharp formed before the Amazonian period. *Earth Planet. Sci. Lett.* **554**, 116667 (2021).
55. C. B. Agee *et al.*, Unique meteorite from early Amazonian Mars: Water-rich basaltic breccia Northwest Africa 7034. *Science* **339**, 780–785 (2013).
56. T. J. Lapen *et al.*, A younger age for ALH84001 and its geochemical link to Shergottite sources in Mars. *Science* **328**, 347–351 (2010).
57. P. B. Niles, L. A. Leshin, Y. Guan, Microscale carbon isotope variability in ALH84001 carbonates and a discussion of possible formation environments. *Geochim. Cosmochim. Acta* **69**, 2931–2944 (2005).
58. R. Shaheen, P. B. Niles, K. Chong, C. M. Corrigan, M. H. Thiemens, Carbonate formation events in ALH 84001 trace the evolution of the Martian atmosphere. *Proc. Natl. Acad. Sci. U.S.A.* **112**, 336–341 (2015).
59. J. J. Barnes *et al.*, Multiple early-formed water reservoirs in the interior of Mars. *Nat. Geosci.* **13**, 260–264 (2020).
60. A. Udry *et al.*, What Martian meteorites reveal about the interior and surface of Mars. *J. Geophys. Res. Planets* **125**, e2020JE006523 (2020).
61. E. B. Rampe *et al.*, Mineralogy and geochemistry of sedimentary rocks and eolian sediments in Gale crater, Mars: A review after six Earth years of exploration with curiosity. *Geochemistry* **80**, 125605 (2020).
62. P. K. Swart, The geochemistry of carbonate diagenesis: The past, present and future. *Sedimentology* **62**, 1233–1304 (2015).
63. R. Hu, D. M. Kass, B. L. Ehlmann, Y. L. Yung, Tracing the fate of carbon and the atmospheric evolution of Mars. *Nat. Commun.* **6**, 10003 (2015).
64. T. B. Thomas, R. Hu, D. Y. Lo, Constraints on the size and composition of the ancient Martian atmosphere from coupled CO_2–N_2–Ar isotopic evolution models. *Planet. Sci. J.* **4**, 41 (2023).
65. C. Jimenez-Lopez, C. S. Romanek, Precipitation kinetics and carbon isotope partitioning of inorganic siderite at 25 °C and 1 atm. *Geochim. Cosmochim. Acta* **68**, 557–571 (2004).
66. T. Chacko, P. Deines, Theoretical calculation of oxygen isotope fractionation factors in carbonate systems. *Geochim. Cosmochim. Acta* **72**, 3642–3660 (2008).
67. W. W. Carothers, L. H. Adami, R. J. Rosenbauer, Experimental oxygen isotope fractionation between siderite-water and phosphoric acid liberated CO2-siderite. *Geochim. Cosmochim. Acta* **52**, 2445–2450 (1988).
68. C. L. Zhang *et al.*, Temperature-dependent oxygen and carbon isotope fractionations of biogenic siderite. *Geochim. Cosmochim. Acta* **65**, 2257–2271 (2001).
69. C. A. M. Brenninkmeijer, P. Kraft, W. G. Mook, Oxygen isotope fractionation between CO_2 and H_2O. *Chem. Geol.* **41**, 181–190 (1983).
70. A. Steele, F. M. McCubbin, M. D. Fries, The provenance, formation, and implications of reduced carbon phases in Martian meteorites. *Meteoritics Planet. Sci.* **51**, 2203–2225 (2016).
71. J. Alday *et al.*, Oxygen isotopic ratios in Martian water vapour observed by ACS MIR on board the exomars trace gas orbiter. *A&A* **630**, A91 (2019).
72. F. Lefèvre, V. Krasnopolsky, "Atmospheric photochemistry" in *The Atmosphere and Climate of Mars*, R. M. Haberle, R. T. Clancy, F. Forget, M. D. Smith, R. W. Zurek, Eds. (Cambridge University Press, 2017), pp. 405–432, 10.1017/9781139060172.013.
73. J. Horita, D. J. Wesolowski, Liquid–vapor fractionation of oxygen and hydrogen isotopes of water from the freezing to the critical temperature. *Geochim. Cosmochim. Acta* **58**, 3425–3437 (1994).
74. R. E. Criss, *Principles of Stable Isotope Distribution* (Oxford University Press, 1999).
75. L. P. Baumgartner, J. W. Valley, Stable isotope transport and contact metamorphic fluid flow. *Rev. Mineral. Geochem.* **43**, 415–467 (2001).
76. Z. Sharp, *Principles of Stable Isotope Geochemistry* (The University of New Mexico, ed. 2, 2017).
77. W. Rapin *et al.*, Sustained wet–dry cycling on early Mars. *Nature* **620**, 299–302 (2023).
78. R. Wordsworth *et al.*, A coupled model of episodic warming, oxidation and geochemical transitions on early Mars. *Nat. Geosci.* **14**, 127–132 (2021).
79. R. Gonfiantini, L. I. Wassenaar, L. Araguas-Araguas, P. K. Aggarwal, A unified CraigGordon isotope model of stable hydrogen and oxygen isotope fractionation during fresh or saltwater evaporation. *Geochim. Cosmochim. Acta* **235**, 224–236 (2018).
80. I. Halevy, W. W. Fischer, J. M. Eiler, Carbonates in the Martian meteorite Allan Hills 84001 formed at 18 4 C in a near-surface aqueous environment. *Proc. Natl. Acad. Sci. U.S.A.* **108**, 16895–16899 (2011).
81. J. Zhang, P. D. Quay, D. O. Wilbur, Carbon-isotope fractionation during gas-water exchange and dissolution of CO2. *Geochim. Cosmochim. Acta* **59**, 107–114 (1995).
82. P. J. Gasda *et al.*, "ChemCam observations of the marker band, Gale crater, Mars" in *54th Lunar and Planetary Science Conference* (Lunar and Planetary Institute, The Woodlands, TX, 2023), vol. 54, p. 2389.
83. C. M. Weitz *et al.*, Orbital observations of a marker horizon at Gale Crater. *J. Geophys. Res. Planets* **127**, e2022JE007211 (2022).
84. C. M. Weitz *et al.*, "The Marker Band in Gale crater: A synthesis of orbital and ground observations" in *54th Lunar and Planetary Science Conference*, (Lunar and Planetary Institute, The Woodlands (TX), 2023), vol. 54, p. 1560.
85. J. R. Allan, R. K. Matthews, "Isotope signatures associated with early meteoric diagenesis" in *Carbonate Diagenesis*, M. E. Tucker, R. Bathurst, Eds. (John Wiley & Sons Ltd, 1990), pp. 197–217.
86. I. D. Clark, B. Lauriol, Kinetic enrichment of stable isotopes in cryogenic calcites. *Chem. Geol.* **102**, 217–228 (1992).
87. D. Lacelle, Environmental setting, (micro)morphologies and stable C-O isotope composition of cold climate carbonate precipitates–A review and evaluation of their potential as paleoclimatic proxies. *Quat. Sci. Rev.* **26**, 1670–1689 (2007).
88. R. A. Socki, P. B. Niles, Q. Fu, E. K. Gibson Jr., "Cryogenic carbonate formation on Mars: Clues from stable isotope variations seen in experimental studies" in *41st Lunar and Planetary Science Conference* (Lunar and Planetary Institute, The Woodlands, TX, 2010).
89. F. J. Martín-Torres *et al.*, Transient liquid water and water activity at Gale crater on Mars. *Nat. Geosci.* **8**, 357–361 (2015).
90. B. M. Jakosky, Atmospheric loss to space and the history of water on Mars. *Annu. Rev. Earth Planet. Sci.* **49**, 71–93 (2021).
91. E. S. Kite, I. Halevy, M. A. Kahre, M. J. Wolff, M. Manga, Seasonal melting and the formation of sedimentary rocks on Mars, with predictions for the Gale Crater mound. *Icarus* **223**, 181–210 (2013).
92. D. Hall, Mineral precipitation in North Slope river icings. *Arctic* **33**, 343–348 (1980).
93. D. Möhlmann, K. Thomsen, Properties of cryobrines on Mars. *Icarus* **212**, 123–130 (2011).
94. Y.-F. Zheng, Oxygen isotope fractionation in carbonate and sulfate minerals. *Geochem. J.* **33**, 109–126 (1999).
95. D. T. Vaniman *et al.*, Mineralogy of a mudstone at Yellowknife Bay, Gale Crater, Mars. *Science* **343**, 1243480 (2014).
96. T. F. Bristow *et al.*, Clay mineral diversity and abundance in sedimentary rocks of Gale crater, Mars. *Sci. Adv.* **4**, eaar3330 (2018).
97. D. Blake *et al.*, Characterization and calibration of the CheMin mineralogical instrument on Mars Science Laboratory. *Space Sci. Rev.* **170**, 341–399 (2012).
98. P. Dera *et al.*, High pressure single-crystal micro X-ray diffraction analysis with GSE_ADA/RSV software. *High Pressure Res.* **33**, 466–484 (2013).
99. S. J. Chipera, D. L. Bish, FULLPAT: A full-pattern quantitative analysis program for X-ray powder diffraction using measured and calculated patterns. *J. Appl. Cryst.* **35**, 744–749 (2002).
100. S. J. Chipera, D. L. Bish, Fitting full X-ray diffraction patterns for quantitative analysis: A method for readily quantifying crystalline and disordered phases. *Adv. Mater. Phys. Chem.* **3**, 47–53 (2013).
101. P. D. Archer Jr. *et al.*, Abundances and implications of volatile-bearing species from evolved gas analysis of the Rocknest aeolian deposit, Gale Crater, Mars. *J. Geophys. Res. Planets* **119**, 237–254 (2014).
102. A. C. McAdam *et al.*, Constraints on the mineralogy and geochemistry of Vera Rubin Ridge, Gale Crater, Mars, from Mars Science Laboratory sample analysis at Mars evolved gas analyses. *J. Geophys. Res. Planets* **125**, e2019JE006309 (2020).
103. C. R. Webster, P. R. Mahaffy, Determining the local abundance of Martian methane and its' 13C/12C and D/H isotopic ratios for comparison with related gas and soil analysis on the 2011 Mars Science Laboratory (MSL) mission. *Planet. Space Sci.* **59**, 271–283 (2011).
104. J. Ward, MSL: SAM (Sample Analysis at Mars). PDS Geosciences Node. https://pds-geosciences.wustl.edu/missions/msl/sam.htm. Accessed 12 June 2024.

Downloaded from https://www.pnas.org by 71.228.158.19 on April 25, 2025 from IP address 71.228.158.19.